Coherence Resonance in the FitzHugh-Nagumo system

Gautam Reddy and Chaitanya Murthy

December 10, 2013

1 Introduction

The simplest models used to describe physical systems are often linear. However, several natural phenomena can only be accurately modeled by relatively complex nonlinear systems of equations. There is a wealth of interesting dynamics displayed by systems consisting of nonlinear elements, for example systems in which the dynamics depend delicately on the initial conditions, *viz*, chaos, and systems which generate fractal structures. These types of dynamics are especially noticeable in models of biological phenomena such as cardiac arrythmia, fluctuations in predator-prey populations, or neuronal cascades in the human brain.

Of special interest to us are the class of nonlinear systems which are *excitable* by external stimuli. Excitability is characterized by a response that is highly nonlinear; for small perturbations, the system remains steady, but once a threshold is reached, the system "spikes", leaving the resting state entirely and going on an excursion in phase space. This type of behavior is characteristic of the action potential train through a neuron, described by the Hodgkin-Huxley (HH) model [1]. In the early 1950s, Hodgkin and Huxley performed action potential measurements on the squid giant axon and proposed a model of action potential transmission, typically represented as an electrical circuit as shown in Figure 1. The classical model of potential transmission through a neuron was of the form

$$C_m \frac{\mathrm{d}V}{\mathrm{d}t} = -\frac{V - V_{eq}}{R} + I_{appl} \tag{1}$$

where C_m is the membrane capacitance, R is the resistance, V is the potential and I_{appl} is the excitation. As evident from the form of the equation, I_{appl} provides an excitation and the potential relaxes back to V_{eq} in a time-scale set by the product $C_m R$, representative of an excitation-relaxation type of behavior. Using experimental data and accounting for both sodium and potassium ion channels, Hodgkin-Huxley proposed a more complex model equation consisting of various nonlinear elements,

$$C_m \frac{\mathrm{d}V}{\mathrm{d}t} = -g_K n^4 (V - V_K) - g_{Na} m^3 h (V - V_{Na}) - g_L (V - V_L) + I_{appl} \tag{2}$$

where $g_K n^4$, $g_{Na} m^3 h$ and g_L are effective conductances of potassium, sodium and leakage channels. n, m and h are dimensionless quantities associated respectively with potassium channel activation, sodium channel activation, and sodium channel inactivation, and obey linear dynamics with coefficients that are potential-dependent, making the model a nonlinear set of equations in four variables.
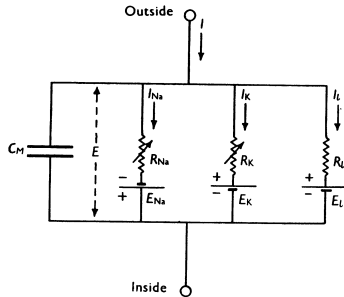

Figure 1: The electrical circuit representing nerve membrane originally proposed by Hodgkin and Huxley (taken from [1])

1.1   The FitzHugh-Nagumo model

The Hodgkin-Huxley model has been hugely successful in describing the transmission of an action potential through a cell membrane. However, due to the large number of variables, the phase space dynamics of the equation is hard to visualize. In 1961, FitzHugh [2] sought to reduce the HH model to a simpler set of equations in two state variables while retaining its essential excitation characteristics. The reduced version was experimentally demonstrated by Nagumo et al [3] using electrical circuits and has since been called the FitzHugh-Nagumo (FN) model (FitzHugh himself called it the *Bonhoeffer-van der Pol model*, for reasons that will soon become clear).

Instead of simply stating the FN equations, it is enlightening to loosely follow FitzHugh's own derivation of his model. We start with an innocuous linear differential equation for a damped oscillator:

$$\ddot{x} + \gamma\dot{x} + x = 0 \tag{3}$$

If we replace the constant damping coefficient by one that depends quadratically on x, we obtain the famous Van der Pol oscillator [4] which has significantly richer dynamics (deterministic chaos and whatnot),

$$\ddot{x} + c(x^2 - 1)\dot{x} + x = 0 \tag{4}$$

Applying the Liénard transformation $y = x - \dot{x}/c - x^3/c$, we can write equation (4) in two-dimensional form:

$$\dot{x} = c(x - x^3/3 - y) \tag{5}$$
$$\dot{y} = x/c \tag{6}$$

Adding one or two extra terms, we arrive at the general deterministic FN model, which may be represented in the following form

$$\epsilon\dot{x} = x - x^3/3 - y + z \tag{7}$$
$$\dot{y} = -\gamma x - \beta y + a \tag{8}$$

These equations are relatively simple mathematically, but they capture the essential *qualitative* properties of a large class of excitable nonlinear systems. Not surprisingly, they are also quite widely studied.

In our discussion, as done in [5], we will work with the particularly simple FN model

$$\epsilon\dot{x} = x - x^3/3 - y \tag{9}$$
$$\dot{y} = x + a \tag{10}$$

2   Dynamics of the deterministic FitzHugh-Nagumo model

The dynamics of a two-dimensional nonlinear system such as equations (9) and (10) is best studied on the *phase plane* spanned by the two dynamic variables x and y. The *phase point* representing the state of the system moves spontaneously in this plane along paths that satisfy the equations of motion. These paths should be thought of as completely filling the plane, like the stream lines of a flowing fluid. There are two special curves on the phase plane, called *nullclines*, along which the velocities of x or y are zero. These are clearly obtained by setting the derivatives in the equations of motion equal to zero. From equations (9) and (10), the x-nullcline is the cubic curve $y = x - x^3/3$, while the y-nullcline is simply the vertical line $x = -a$. The qualitative behavior of the system for different parameter values can generally be inferred just by plotting the nullclines and looking at the overall structure of the flow field. In Figure 2, we show the phase portraits for $a = 1.05$ and $a = 0.95$ respectively.
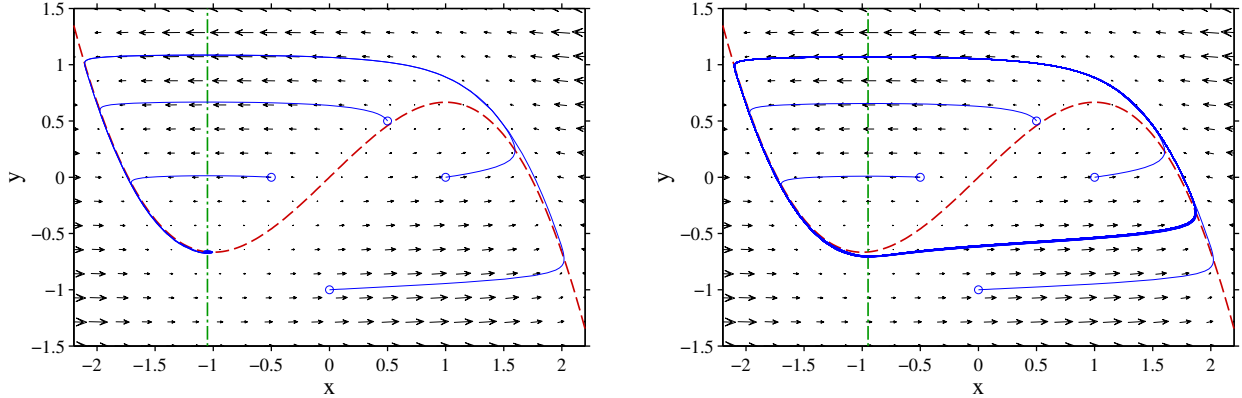
Figure 2: Phase portraits for the deterministic FN model. The red and green dashed lines are the x- and y-nullclines respectively. The black arrows show the velocity field. Representative trajectories are shown in blue, with their origins marked by circles. The figure on the left is for $\epsilon = 0.05, a = 1.05$, while that on the right is for $\epsilon = 0.05, a = 0.95$

Suppose our initial point is $(-0.5, 0)$ and $\epsilon = 0.05$. For $a > 1$, the dynamics proceeds as follows - the system first moves to the left branch of the x-nullcline and slides downwards along the curve onto the point where the two nullclines intersect, i.e., at $(x, y) = (-a, -\frac{a^3}{3} + a)$. This fixed point is stable and by symmetry, the system has a stable fixed point for $|a| > 1$. The dynamics are more interesting for $|a| < 1$, however. The system moves from the initial point to the left branch and slides down it. However, once it reaches the bottom-most point of the curve, the velocity in the y-direction pushes it out of the x-nullcline, thereby destablizing x-motion. Due to the small value of ϵ, velocities off the nullclines greatly favor horizontal motion. The system now makes a jump to the other branch of the x-nullcline, where x motion is stabilised once more, and proceeds to move up the curve. At the top of the curve, the system makes another jump onto the left branch. The process repeats and we observe a *limit cycle*.

In the next section, we introduce a noise term, making the dynamics even more exciting.

3   Coherence resonance in the FitzHugh-Nagumo system

3.1   The stochastic FitzHugh-Nagumo model

The deterministic equations of motion for the FN model can be made stochastic in the following simple manner:

$$\epsilon \dot{x} = x - x^3/3 - y \tag{11}$$

$$\dot{y} = x + a + D\xi(t) \tag{12}$$

Here, the parameter D governs the amplitude of the noisy external force ξ, which is taken to be Gaussian delta-correlated with zero mean $\langle \xi(t)\xi(t') \rangle = \delta(t - t')$. As mentioned in [5], noise in equation (12) can be interpreted directly as fluctuations of the bifurcation parameter a, which in turn switches the limit cycle on and off. There is no equivalent obvious interpretation for noise added directly to equation (11).

The discretization of these equations, to first order in Δt, is

$$x(t + \Delta t) = x(t) + \left[x(t) - \frac{x(t)^3}{3} - y(t) \right] \frac{\Delta t}{\epsilon} \tag{13}$$

$$y(t + \Delta t) = y(t) + \left(x(t) + a \right) \Delta t + (\sqrt{\Delta t}D)W_1 \tag{14}$$

where W_1 is a Gaussian random variable with mean zero and variance one. This is Euler's method for simulating stochastic differential equations, and is the method used in the original paper by Pikovsky and Kurths [5]. The results presented here were obtained from simulations using this scheme.

3

3.2 Simulations

We simulated the FitzHugh-Nagumo model using MATLAB (see Appendix B for codes), for the parameters $\epsilon = 0.01$, $a = 1.05$, and a range of different noise amplitudes D. These parameters were chosen so that we could reproduce the results of [5]. Representative results from our simulations are presented in Figure 3 below (compare Figs. 1, 2 in [5]). The phenomenon of *coherence resonance* is qualitatively visible in the figures on the left; the noise-excited oscillations are maximally coherent for moderate noise, becoming more irregular for larger or smaller noise amplitudes.
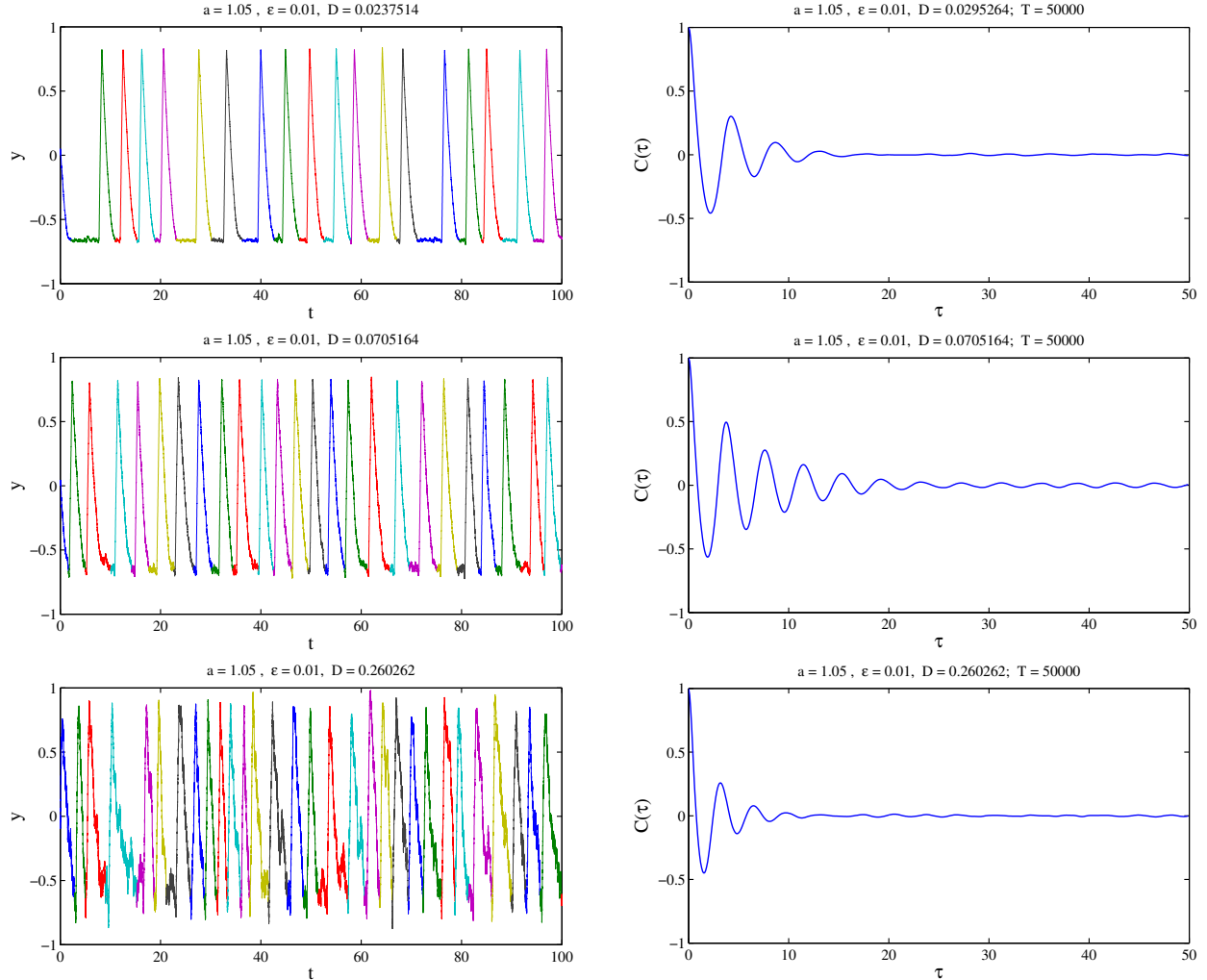

Figure 3: Simulated dynamics of the FN system. Left panel: time-series of y for model parameters $a = 0.95$, $\epsilon = 0.01$ and varying noise amplitudes (from top to bottom $D \approx 0.02, 0.07$ and 0.26). Each color represents one pulse (the pulse durations are used to calculate the noise-to-signal ratio R). Right panel: corresponding autocorrelation functions at the given noise levels. The quantity T is the total length of each simulation in arbitrary time units.

We calculated the normalized autocorrelation function over a long time period for each set of parameters:

$$C(\tau) = \frac{\langle \tilde{y}(t)\tilde{y}(t+\tau)\rangle}{\langle \tilde{y}^2 \rangle}, \qquad \tilde{y}(t) \equiv y(t) - \langle y \rangle \tag{15}$$

These functions are plotted on the right side of Figure 3. They also reproduce the results of Pikovsky and Kurths well, and again demonstrate the coherence resonance (correlations decay slower for moderate noise).
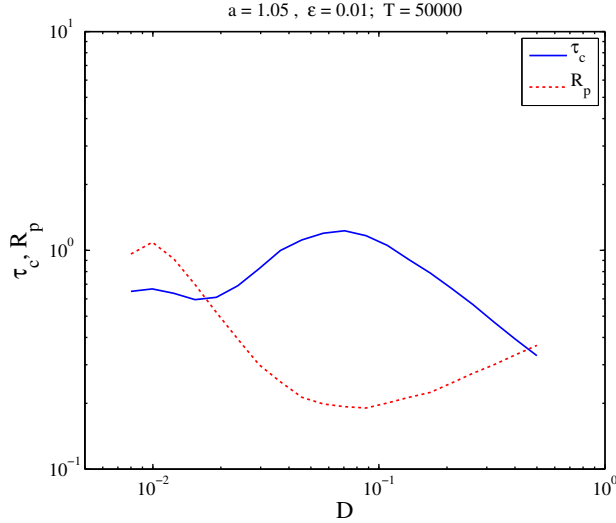
4

Figure 4: Correlation time τ_c (blue solid line) and noise-to-signal ratio R_p (red dotted line) vs. noise amplitude D for the FN system with $a = 0.95$ and $\epsilon = 0.01$

The rate at which the autocorrelation function decays can be described neatly with a single quantity, the characteristic correlation time, defined as

$$\tau_c = \int_0^\infty C^2(t)dt \tag{16}$$

We computed τ_c by numerically integrating the obtained correlation functions according to the trapezoid rule for each simulated noise amplitude. The dependence is shown in Figure 4, and displays a marked peak at $D \approx 0.06$.

We can also characterize the coherence resonance via a different quantity. The process depicted on the left of Figure 3 can be readily viewed as a sequences of pulses, each having a duration t_p. The normalized fluctuations of pulse durations,

$$R_p = \frac{\sqrt{\langle t_p{}^2 \rangle - \langle t_p \rangle^2}}{\langle t_p \rangle} \tag{17}$$

which can be interpreted as the noise-to-signal ratio, shows a minimum at the same noise amplitude $D \approx 0.06$ at which the correlation time shows a maximum (see Figure 4).

4   Fokker-Planck equation and stationary probability density

The Fokker-Planck equation (FPE) for the probability density $P(x, y, t | x_0, y_0, t_0)$, corresponding to the system of equations equations (11) and (12) describing the stochastic FN model is

$$\frac{\partial P}{\partial t} = -\frac{1}{\epsilon} \frac{\partial}{\partial x} \left[\left(x - \frac{x^3}{3} - y \right) P \right] - \frac{\partial}{\partial y} \left[(x + a) P \right] + \frac{D^2}{2} \frac{\partial^2 P}{\partial y^2} \tag{18}$$

Note that the parameter D here is not the diffusion constant. Unfortunately, this FPE does not seem to be solvable analytically, even in the stationary case [6]. Under some fairly restrictive set of conditions and approximations, an exact nonequilibrium potential *has* been obtained by Izús et al. [7], but their approach is far beyond the scope of this report. The stationary probability distribution for this FPE has been probed extensively via numerical simulations, starting with the work of Treutlein and Schulten [8] in the 1980s. Instead of resorting to full-blown finite-element simulations, we will instead follow the semi-analytical method of Lindner and Schimansky-Geier [9].

The FN problem becomes tractable in the limit of small ϵ, which corresponds to a large separation of time-scales between the variables x and y. In this limit, the fast variable x relaxes very quickly towards one of the stable branches of the nullcline $y = x - x^3/3$. The cubic function can be inverted to give x as a function of y along the left and right branches,

$$x_L(y) = 3y_- \cos\left(\frac{1}{3}\arccos\left(y/y_+\right)\right) \tag{19}$$

$$x_R(y) = 3y_+ \cos\left(\frac{1}{3}\arccos\left(y/y_-\right)\right) \tag{20}$$

where the trigonometric functions are understood to go over to their hyperbolic counterparts if the innermost argument is greater than 1.

In the $\epsilon \to 0$ limit, the two-dimensional stochastic process described by equation (18) therefore *separates into two one-dimensional processes*, occurring on the right and left branches, and coupled by probability currents $J_{R\to L}$ and $J_{L\to R}$ (see Figure 5 below). Since jumps between branches occur instantaneously in the $\epsilon \to 0$ limit, there is no finite probability density on the straight lines l_2 and l_1 along which these currents flow.

Thus, we obtain two coupled FPEs in the slow variable y,

$$\frac{\partial P_L}{\partial t} = \frac{\partial}{\partial y}\left[-a - x_L(y) + \frac{D^2}{2}\frac{\partial}{\partial y}\right]P_L + J_{R\to L}\delta(y - y_+) \tag{21}$$

$$\frac{\partial P_R}{\partial t} = \frac{\partial}{\partial y}\left[-a - x_R(y) + \frac{D^2}{2}\frac{\partial}{\partial y}\right]P_R + J_{L\to R}\delta(y - y_-) \tag{22}$$

describing the evolution of the probability density on the left and right branches. P_L and P_R are defined on the semi-infinite intervals $[y_-, \infty)$ and $(-\infty, y_+]$ respectively, and $x(y)$ is the inverse of the cubic function along the appropriate branch. Absorbing boundaries at the finite endpoints of each interval account for probability *outflow* to the other branch, and the delta-function terms in the FPEs represent the corresponding probability *inflows*. Since $P(y)$ vanishes at the absorbing boundaries, we have

$$J_{L\to R} = \left.\frac{D^2}{2}\frac{\partial P_L}{\partial y}\right|_{y=y_-} \qquad \text{and} \qquad J_{R\to L} = \left.-\frac{D^2}{2}\frac{\partial P_R}{\partial y}\right|_{y=y_+} \tag{23}$$

Of course, the total probability in the system must be conserved

$$\int_{y_-}^{\infty} P_L(y)\,\mathrm{d}y + \int_{-\infty}^{y_+} P_R(y)\,\mathrm{d}y = 1 \tag{24}$$
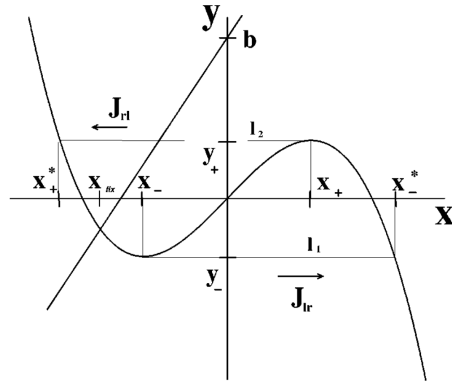

Figure 5: Nullclines of the system and some particular points used in the derivations. This diagram was taken from [9], who used a slightly different form of the FN model; hence the slanted y-nullcline and other small discrepancies.

6

At steady-state, the probability current must also be constant and equal to the average pulse rate

$$J_{L \to R} = J_{R \to L} = r \tag{25}$$

The stationary solutions of the coupled FPEs (equations (21) and (22)) are

$$P_L(y) = \frac{2r}{D^2} \int_{y_-}^{y} \mathrm{d}z \, e^{2[U_L(z) - U_L(y)]/D^2} \Theta(y_+ - z) \tag{26}$$

$$P_R(y) = \frac{2r}{D^2} \int_{y}^{y_+} \mathrm{d}z \, e^{2[U_R(z) - U_R(y)]/D^2} \Theta(z - y_-) \tag{27}$$

with the effective potentials $U_L(y)$ and $U_R(y)$ given by

$$U_L(y) = -ay - \frac{x_L(y)}{4} \left[3y - x_L(y)\right] \tag{28}$$

$$U_R(y) = -ay - \frac{x_R(y)}{4} \left[3y - x_R(y)\right] \tag{29}$$

For the detailed derivation of these results, see Appendix A. The remaining free variable in equations (26) and (27) is the pulse rate r, which is then determined by the normalization condition of equation (24).

We compare the approximate analytical probability distributions obtained in equations (26) and (27) to those obtained by averaging over direct simulations of the Langevin equations (11) and (12). The approximation remains accurate up to values of $\epsilon \approx 0.01$, as the results in Figure 6 below indicate.
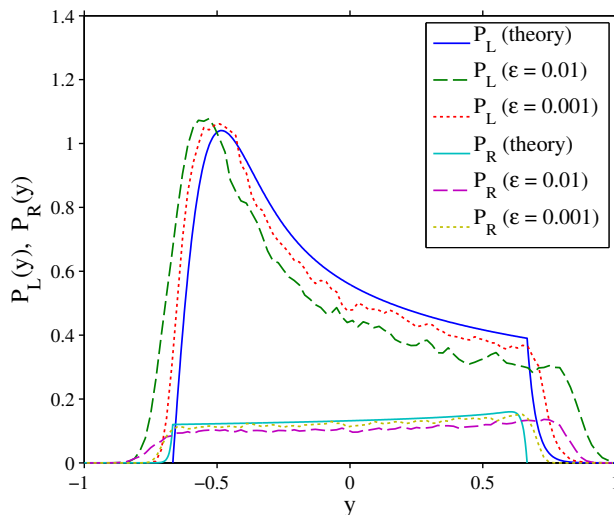

Figure 6: The probability densities on the right and left branch are computed for $a = 1.05$ and $D = 0.25$. The approximation (theory), formally valid in the limit $\epsilon \to 0$, is compared to distributions obtained by averaging over simulations performed with finite values of ϵ.

5 Simple prototype for coherence resonance

To construct a simple prototype for coherence resonance, we reduce the dynamics of the two variable system on the slow branch to a one-dimensional Langevin equation. In the slow region of phase space, the system is restricted to the x-nullcline. As described above, on this line x can be written as a function of y. Plugging it back into the equation for y, we have

$$\frac{dy}{dt} = -\frac{dU}{dy} + D\xi(t) \tag{30}$$

7

where $-\frac{dU}{dy}$ is x in terms of y. The above equation simulates the behavior of y on one branch. To describe the complete behavior, we define the above equation on the negative y axis (y ranges from $-\infty$ to 0). y initializes at a chosen point y_0 and evolves stochastically to zero, provided we choose an appropriate U. Since coherence resonance is observed in the parameter range with a stable fixed point, we need U to have a minimum close to the excitation region. The system occasionally escapes from the well and reaches zero with a rate that depends on the amplitude of the noise. The region $y \geq 0$ is the excitation region, i.e. y jumps from one slow branch to another. In our simplified prototype model, we reset y to y_0 and repeat the procedure, effectively simulating quasiperiodicity.

To show that such a reduction emulates the behavior of the FitzHugh-Nagumo system, we calculate the characteristic correlation times and the noise-to-signal ratio for the prototype. The potential chosen was

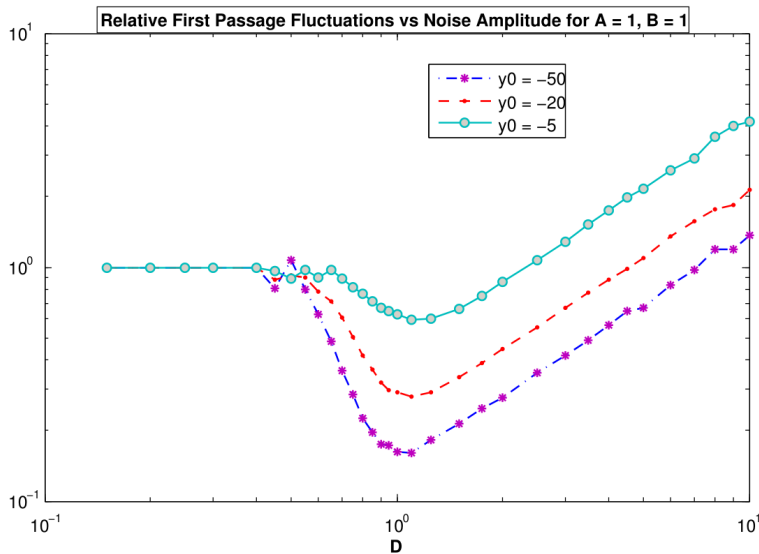$$U(y) = \begin{cases} -Ay, & \text{if } y < -1 \\ A + B + By, & \text{if } -1 \leq y \leq 0 \end{cases} \tag{31}$$

Figure 7: Relative first passage time fluctuations R vs noise amplitude D for $A = B = 1$ and different reinjection points y_0. R may equivalently be interpreted as the noise-to-signal ratio.

The plots in Figure 7 show the noise-to-signal ratio versus noise amplitude for different y_0. In our simulations we use $A = 1$ and $B = 1$. Changing the potential to a harmonic potential or changing the A and B does not change the qualitative nature of the dynamics.

From this prototype, we can extract the essential ingredients necessary for coherence resonance. Firstly, there should be a stable fixed point close to the excitation point. Secondly, upon reaching excitation i.e., $y = 0$, the system should effectively reset itself to an earlier point y_0. Lastly, the noise amplitude must be large enough that the system can escape from the fixed point, but not so large as to cause significant irregular motion during the return journey (which would lead to quasiperiodic rather than periodic behavior).

6 Concluding remarks

Coherence resonance is a fascinating nonlinear phenomenon exhibited by certain excitable models in the presence of purely stochastic forcing. We have studied this behavior in the FitzHugh-Nagumo model, both via direct simulations of the stochastic equations of motion and by considering the system's Fokker-Planck equation in a particular limit where the dynamics may be effectively described in one dimension. We have closely followed the methods described in several excellent papers on the subject, which are listed in the references. We have also included most of the simulation codes that we wrote for this project (Appendix B), in the hope that others will enjoy using them to explore this interesting model and phenomenon.

References

[1] AL Hodgkin and AF Huxley. "A quantitative description of membrane current and its application to conduction and excitation in nerve". In: *The Journal of physiology* 117.4 (1952), pp. 500–544. URL: http://www.ncbi.nlm.nih.gov/pmc/articles/pmc1392413/.

[2] Richard FitzHugh. "Impulses and Physiological States in Theoretical Models of Nerve Membrane". In: *Biophysical Journal* 1.6 (July 1961), pp. 445–466. ISSN: 00063495. DOI: 10.1016/S0006-3495(61)86902-6. URL: http://linkinghub.elsevier.com/retrieve/pii/S0006349561869026.

[3] J Nagumo, S Arimoto, and S Yoshizawa. "An active pulse transmission line simulating nerve axon". In: *Proceedings of the IRE* 50.10 (1962), pp. 2061–2070. URL: http://ieeexplore.ieee.org/xpls/abs_all.jsp?arnumber=4066548.

[4] Balth Van der Pol. "LXXXVIII. On relaxation-oscillations". In: *The London, Edinburgh, and Dublin Philosophical Magazine and Journal of Science* 2.11 (1926), pp. 978–992.

[5] Arkady Pikovsky and Jürgen Kurths. "Coherence Resonance in a Noise-Driven Excitable System". In: *Physical Review Letters* 78.5 (Feb. 1997), pp. 775–778. ISSN: 0031-9007. DOI: 10.1103/PhysRevLett.78.775. URL: http://link.aps.org/doi/10.1103/PhysRevLett.78.775.

[6] B Lindner et al. "Effects of noise in excitable systems". In: *Physics Reports* 392.6 (Mar. 2004), pp. 321–424. ISSN: 03701573. DOI: 10.1016/j.physrep.2003.10.015. URL: http://linkinghub.elsevier.com/retrieve/pii/S0370157303004228.

[7] GG Izus, RR Deza, and HS Wio. "Exact nonequilibrium potential for the FitzHugh-Nagumo model in the excitable and bistable regimes". In: *Physical Review E* 58.1 (1998), pp. 93–98. URL: http://pre.aps.org/abstract/PRE/v58/i1/p93_1.

[8] Herbert Treutlein and Klaus Schulten. "Noise Induced Limit Cycles of the Bonhoeffer-Van der Pol Model of Neural Pulses". In: *Berichte der Bunsengesellschaft für physikalische Chemie* 89.6 (1985), pp. 710–718.

[9] B Lindner and L Schimansky-Geier. "Analytical approach to the stochastic FitzHugh-Nagumo system and coherence resonance." In: *Physical review. E, Statistical physics, plasmas, fluids, and related interdisciplinary topics* 60.6 Pt B (Dec. 1999), pp. 7270–6. ISSN: 1063-651X. URL: http://www.ncbi.nlm.nih.gov/pubmed/11970671.

A Derivation of stationary probability distribution

Looking for stationary solutions $P_L(y,t) = P_L(y)$, we set the LHS of equation (21) to zero and integrate once to obtain

$$r = -\left[a + x_L(y)\right]P_L + \frac{D^2}{2}\frac{\partial P_L}{\partial y} + r\Theta(y - y_+) = constant \tag{32}$$

where $\Theta(x - x_0) = \int_{-\infty}^{x} \mathrm{d}z\,\delta(z - x_0)$ is the unit step function. Rearranging,

$$\frac{\partial P_L}{\partial y} - \frac{2\left[a + x_L(y)\right]}{D^2}P_L = \frac{2r}{D^2}\Theta(y_+ - y) \tag{33}$$

Define the integrating factor

$$\psi(y) = \exp\left\{-\frac{2}{D^2}\int_{y_-}^{y}\mathrm{d}y'\left[x_L(y') + a\right]\right\} \tag{34}$$

The integral is easily carried out by using $y = x - x^3/3 \Rightarrow \mathrm{d}y = \mathrm{d}x\left(1 - x^2\right)$:

$$
\begin{aligned}
U_L(y) &\equiv -\int_{y_-}^{y}\mathrm{d}y'\left[x_L(y') + a\right] \\
&= -ay - \int_{-1}^{x_L(y)}\mathrm{d}x\left(x - x^3\right) \\
&= -ay - \frac{x_L(y)^2}{2} + \frac{x_L(y)^4}{4} \\
&= -ay - \frac{x_L(y)}{4}\left[3y - x_L(y)\right]
\end{aligned} \tag{35}
$$

where constant terms have been ignored since they will cancel in the final solution.

Multiplying equation (33) by $\psi(y) = e^{2U_L(y)/D^2}$ transforms the LHS into a total derivative, so we immediately obtain the solution

$$P_L(y) = \frac{2r}{D^2}e^{-2U_L(y)/D^2}\int_{y_-}^{y}\mathrm{d}z\,e^{2U_L(z)/D^2}\Theta(y_+ - z) \tag{36}$$

Following the same procedure starting from equation (22), we obtain the distribution on the right branch.

B MATLAB simulation codes

Three different codes are included. These were created and used with MATLAB 2012b. The simulations may take a long time to run with the given parameter specifications, so it is advised that you change the parameters and/or modify the codes as needed before running them.

The included codes are:

- `fitzHugh_trajectory.m` — traces a trajectory of the FN system in the phase plane.

- `fitzHugh.m` — runs simulations for each of the specified noise strengths D. Generates the equivalent of Figure 3 for each simulation, along with one Figure 4 for the entire set.

- `fitzHugh_probability_density.m` — computes numerically the approximate stationary probability densities given by equations (26) and (27), and compares these to the densities obtained from direct simulation of the FN model for different values of ϵ. Generates the equivalent of Figure 6.